

pubs.acs.org/JACS Article

# Hybrid Bonding Bottlebrush Polymers Grafted from a Supramolecular Polymer Backbone

Tristan D. Clemons, Simon A. Egner, Joseph Grzybek, Joshua J. Roan, Hiroaki Sai, Yang Yang, Zois Syrgiannis, Hao Sun, Liam C. Palmer, Nathan C. Gianneschi, and Samuel I. Stupp\*



Cite This: J. Am. Chem. Soc. 2024, 146, 16085-16096



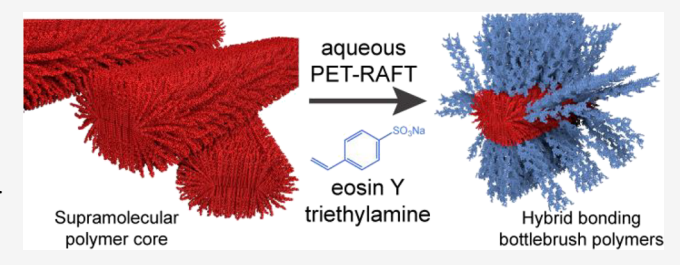
**ACCESS** I

III Metrics & More

Article Recommendations

s) Supporting Information

ABSTRACT: Bottlebrush polymers, macromolecules consisting of dense polymer side chains grafted from a central polymer backbone, have unique properties resulting from this well-defined molecular architecture. With the advent of controlled radical polymerization techniques, access to these architectures has become more readily available. However, synthetic challenges remain, including the need for intermediate purification, the use of toxic solvents, and challenges with achieving long bottlebrush architectures due to backbone entanglements. Herein, we report



hybrid bonding bottlebrush polymers (systems integrating covalent and noncovalent bonding of structural units) consisting of poly(sodium 4-styrenesulfonate) (p(NaSS)) brushes grafted from a peptide amphiphile (PA) supramolecular polymer backbone. This was achieved using photoinitiated electron/energy transfer-reversible addition—fragmentation chain transfer (PET-RAFT) polymerization in water. The structure of the hybrid bonding bottlebrush architecture was characterized using cryogenic transmission electron microscopy, and its properties were probed using rheological measurements. We observed that hybrid bonding bottlebrush polymers were able to organize into block architectures containing domains with high brush grafting density and others with no observable brushes. This finding is possibly a result of dynamic behavior unique to supramolecular polymer backbones, enabling molecular exchange or translational diffusion of monomers along the length of the assemblies. The hybrid bottlebrush polymers exhibited higher solution viscosity at moderate shear, protected supramolecular polymer backbones from disassembly at high shear, and supported self-healing capabilities, depending on grafting densities. Our results demonstrate an opportunity for novel properties in easily synthesized bottlebrush polymer architectures built with supramolecular polymers that might be useful in biomedical applications or for aqueous lubrication.

## **■ INTRODUCTION**

Molecular bottlebrushes, which consist of a long polymeric backbone densely grafted with side chains, possess unique physical and material properties compared to their linear counterparts. 1-3 Proteoglycans in living organisms such as lubricin, which possesses bottlebrush architecture, play many roles from lubrication and shock absorption in joints to scaffolding and cell signaling during development.<sup>4-6</sup> Due to their remarkable properties, polymer chemists have sought to replicate the bottlebrush architecture of these macromolecules primarily using reversible-deactivation radical polymerization (RDRP),<sup>3</sup> and ring-opening polymerization reactions.<sup>7,8</sup> Molecular bottlebrushes can be obtained through three main synthetic approaches: "grafting through" (polymerization of macromonomers), "grafting to" (attachment of polymer side chains to a backbone), and "grafting from" (polymerization of monomers from a backbone) procedures. Each of these methods offers advantages and disadvantages; however, in all cases, careful consideration of steric barriers, reaction conditions, and grafting efficiencies are necessary to achieve high grafting densities and long backbones.<sup>9</sup>

Reversible addition—fragmentation chain transfer (RAFT), 10,11 atom transfer radical polymerization (ATRP), 12–15 nitroxide-mediated polymerization (NMP), 16 and ring-opening metathesis polymerization (ROMP) 17,18 have all been reported for the synthesis of well-defined bottlebrush architectures. These molecular bottlebrushes have been employed as novel drug delivery vehicles, 17–19 bioimaging agents, 15,20 and in industrial applications including lubrication, 12,21 wear resistance, 13 and photonic crystals. 22 These procedures typically require intermediate purification steps such as backbone purification and the use of toxic organic solvents or are hampered by low grafting densities resulting from backbone entanglements. 23 These challenges limit the size and scale achievable for covalent molecular bottlebrush

Received: March 7, 2024 Revised: May 17, 2024 Accepted: May 20, 2024 Published: June 4, 2024





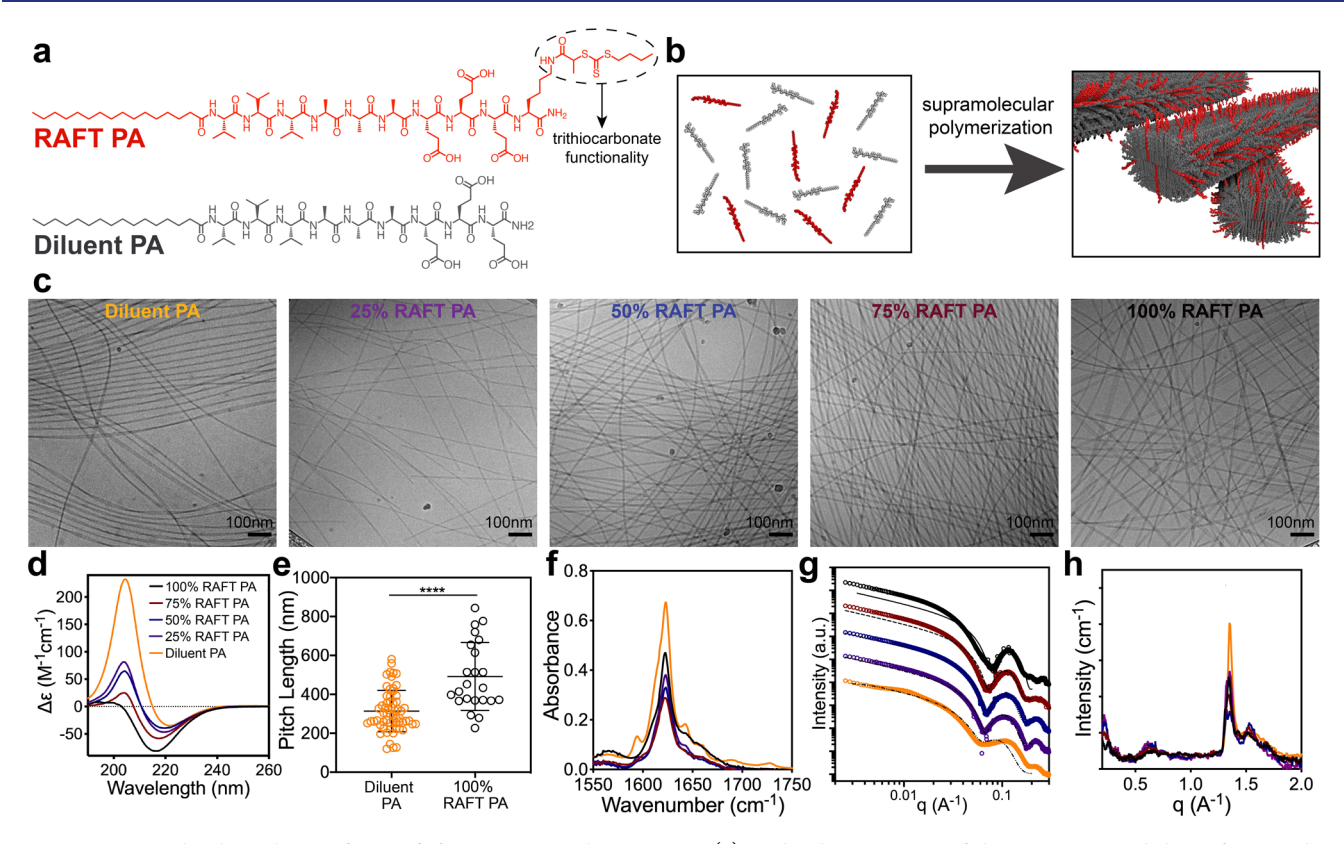


Figure 1. Supramolecular polymers for "graft from" RAFT polymerization. (a) Molecular structures of the RAFT PA and the unfunctionalized diluent PA. (b) Schematic representation of the coassembly of PA molecules into supramolecular nanostructures. (c) Cryogenic transmission electron microscopy, and (d) circular dichroism spectroscopy of the coassembled supramolecular polymers with 0, 25, 50, 75, and 100 mol % of RAFT PA relative to the diluent PA. (e) Pitch length analysis for the diluent PA and 100% RAFT PA supramolecular polymers from representative cryo-TEM micrographs. (f) Fourier transform infrared spectra, (g) small-angle X-ray scattering pattern (overlaid with corresponding core—shell cylinder model (dashed lines)), and (h) wide-angle X-ray scattering scans of coassembled supramolecular polymers. Panel (e) data displayed as mean  $\pm$  s.d.,  $n_{min}$  per group = 25 with an unpaired Student t test used for statistical analysis between groups, significance,  $p < 0.0001^{****}$ .

polymers. Furthermore, many of these chemistries have focused on covalent carbon—carbon linkages in both the backbone and brush chains. This creates a macromolecule of high molecular weight with limited degradation possibilities, a concern considering the significant problem of persistent plastic pollution in the natural environment. 24–26

One way to overcome the challenges of bottlebrush polymer synthesis is to combine both covalent and noncovalent bonds among structural units to create hybrid bonding bottlebrush polymers with a significant degree of noncovalency (DNC).<sup>27</sup> Supramolecular polymers, such as those made from peptide amphiphiles (PAs), can form high-persistence-length nanofibers with minimal chain entanglement, resulting from the combination of both strong intermolecular monomer cohesion and a high degree of surface charge repulsion. This provides an ideal platform for achieving molecular bottlebrush architectures through a hybrid bonding polymer approach that makes use of both supramolecular and covalent polymerization techniques.<sup>28</sup> Manners and co-workers have developed a number of unique polymeric bottlebrush architectures resulting from block copolymers undergoing a living crystallization-driven self-assembly process.<sup>29-32</sup> These hybrid macromolecules, which can be tuned to many microns in length,<sup>30</sup> have potential applications in cellular delivery and targeting,<sup>29</sup> and in surface-initiated polymerizations to construct functional bottlebrush-tethered surfaces.<sup>31</sup> Brendel and co-workers have investigated supramolecular polymer bottlebrushes by precisely studying the interplay of traditional

supramolecular assembly motifs coupled to amphiphilic covalent polymers. 33-35 In a recent example, they demonstrated the self-assembling capabilities of benzene trisurea groups tethered to amphiphilic copolymers to drive formation of a supramolecular bottlebrush architecture. Similarly, Perrier and co-workers have extensively studied the use of self-assembling cyclic peptide polymer conjugates for the preparation of supramolecular bottlebrush architectures.

In 2016, the Perrier group compared the efficacy between "graft from" and "graft to" polymerization approaches to produce cyclic peptide-polymer conjugates.<sup>38</sup> These conjugates were first synthesized in organic solvents and then transferred to an aqueous environment to promote assembly of the supramolecular polymer backbone of cyclic peptides to produce the bottlebrush architecture. These studies focused on supramolecular assembly after brush polymer synthesis or conjugation, requiring intermediate purification and solvent extraction. This approach also places constraints on the length of the covalent polymer brush. Longer brush lengths interrupt the supramolecular polymerization mechanism of the backbone, so either backbone length or polymer brush length must be sacrificed. The ability to achieve long backbone assemblies coupled with high molecular weight polymer brushes remains challenging.

In this work, we developed a hybrid bonding bottlebrush polymer platform that makes use of a peptide amphiphile (PA)-based supramolecular polymer backbone with a covalent polymer grafted from this assembly. To achieve this, PET-

RAFT polymerization was employed using trithiocarbonate-functionalized supramolecular polymers to achieve graft from controlled covalent polymerization. This method allowed for the facile preparation of hybrid bonding bottlebrush polymers in an aqueous environment. The resulting macromolecules were extensively characterized by cryogenic transmission electron microscopy (cryoTEM), and the effect of grafting density and brush length on solution rheological properties was assessed.

## RESULTS AND DISCUSSION

Design of RAFT-Functionalized Supramolecular Polymers. To achieve covalent polymerization grafted from a supramolecular polymer, we first designed a PA monomer suitable for supramolecular polymerization that would also display the chain transfer agent functionality necessary for RAFT polymerization. This PA consisted of a palmitic acid "tail" conjugated to three valine and three alanine residues to promote intermolecular  $\beta$ -sheet hydrogen bonding and finally three glutamic acid residues to impart aqueous solubility and amphiphilicity to the molecules. A trithiocarbonate, 2-(butylthiocarbonothioylthio) propanoic acid (BTPA), was coupled to the  $\varepsilon$ -amino group of a terminal lysine residue suitable for the growth of covalent polymer chains by RAFT polymerization from the supramolecular polymer backbone (Figure 1a, see Supporting Information for complete methods). This molecule could be coassembled with a PA lacking chain transfer functionality, the diluent PA, to form supramolecular assembled nanoribbons of varying RAFT agent density along the supramolecular polymer backbone (Figure 1b). This supramolecular copolymerization could, in principle, yield variations in the density of brush chains in the hybrid structures. Nuclear magnetic resonance (NMR, <sup>1</sup>H, and <sup>13</sup>C) spectroscopy indicated stability of the trithiocarbonate chain transfer agent through the solid-phase peptide synthesis (Figure S1), while liquid chromatography mass spectrometry (LC-MS) demonstrated that a high degree of purity was achieved for both the RAFT PA and the diluent PA (Figure S2). Ultraviolet-visible spectroscopy (UV-vis) of the purified RAFT PA indicated a characteristic absorbance band at 315 nm, confirming the presence of the trithiocarbonate functionality (Figure S3).

We next prepared a range of coassemblies of the functionalized RAFT PA with the unfunctionalized diluent PA to tune the amount of chain transfer agent functionality along the supramolecular polymer backbone (25, 50, 75, and 100 mol % RAFT PA). Individual molecules were first codissolved at the desired molar coassembly ratios in hexafluoroisopropanol (HFIP) to disrupt any hydrogen bonding among molecules resulting from purification and to encourage molecular coassembly. Following removal of HFIP by evaporation, the samples were dissolved in 30 mM NaCl, pH adjusted to pH 7.4 with aqueous NaOH, and annealed at 80 °C for 30 min followed by slowly cooling to produce the coassembled supramolecular polymers. This annealing and slow cooling allow the monomers of the supramolecular polymers to acquire greater internal order within the nanoscale filaments they form and approach thermodynamic equilibrium. Annealing can also further elongate the supramolecular polymers and avoid kinetically trapped states. Cryogenic transmission electron microscopy (cryoTEM) revealed the formation of ribbon-shaped supramolecular polymers at all coassembly ratios, suggesting the introduction of the chain

transfer agent functionality in some of the monomers does not interfere with supramolecular polymerization of the PA monomers (Figure 1c).

To investigate the internal arrangement of molecules within the supramolecular polymer, circular dichroism (CD) spectroscopy was used to assess the presence of the peptide secondary structure. For all supramolecular polymer coassemblies, the intensity of peaks associated with a  $\beta$ -sheet secondary structure were observed to decrease with increasing RAFT PA content in the coassembly (Figure 1d). Interestingly, the minima position of the CD spectra appeared to red shift with decreasing amounts of RAFT PA in the supramolecular polymers (Figure S4). This red shift has been shown previously to be associated with an increase in the twist of the  $\beta$ -sheet structure of PAs compared to the canonical  $\beta$ -sheet arrangement.<sup>39,40</sup> To investigate this twisting further, we carried out measurements of the pitch length and fiber width from representative cryoTEM micrographs of the diluent and 100% RAFT PA supramolecular polymers. We did not observe a significant difference in fiber width among samples (Figure S5). However, the pitch length for the diluent PA (310  $\pm$  100 nm) was significantly smaller than that observed for 100% RAFT PA (490  $\pm$  180 nm, Figure 1e). This difference in pitch length equates to a twist per molecule of 0.53° for the diluent PA and 0.34° for the RAFT PA supporting the hypothesis of the red shifts observed by CD spectroscopy. Fourier transform infrared spectroscopy (FTIR) further confirmed the presence of a  $\beta$ -sheet secondary structure in the supramolecular assemblies as indicated by a strong amide-I vibrational band at 1625 cm<sup>-1</sup> (Figure 1f).<sup>4</sup>

Solution-phase X-ray scattering techniques using synchrotron radiation allowed us to characterize the morphology and internal ordering of the supramolecular polymers. In smallangle X-ray scattering (SAXS) scans (see Figure 1g), we observed a slope in the low-q region of approximately -1, consistent with the presence of elongated, one-dimensional assemblies. 42 Interestingly, the minima position for the coassemblies shifted gradually from  $q = 0.063 \text{ Å}^{-1}$  for the diluent PA (0% RAFT PA) to  $q = 0.09 \text{ Å}^{-1}$  for the 100% RAFT PA suggesting a narrowing in the width of the nanoscale assemblies with increasing RAFT PA inclusion. To probe this further, the scattering for each sample was modeled with a core—shell cylinder model (Figure 1g and Table S1). Modeling of the diluent PA supramolecular polymer indicated a width of 50.5 Å in comparison to the 100% RAFT PA supramolecular polymer with a modeled width of 40.5 Å. We attribute this narrowing of nanoribbon width with increasing RAFT PA to the reduced twisting observed by cryoTEM and CD spectroscopy, as described earlier. This results in a more twisted nanoribbon with a larger average cross-sectional area compared with that of a less twisted assembly. Wide-angle X-ray scattering (WAXS) measurements were used to characterize internal order in the coassemblies. At all coassembly ratios, a scattering peak was observed at approximately  $q = 1.33 \text{ Å}^{-1}$ , which corresponds to a d-spacing of 4.72 Å consistent with  $\beta$ sheet hydrogen bonding occurring among molecules within the supramolecular polymers (Figure 1h). Taken together, these results confirm that the presence of varying amounts of chain transfer agent functionality does not prevent the supramolecular polymerization of PA monomers into elongated nanoribbons. We hypothesized that these structures would offer a facile route to graft covalent polymers using RAFT polymerization for the synthesis of hybrid bonding bottlebrush

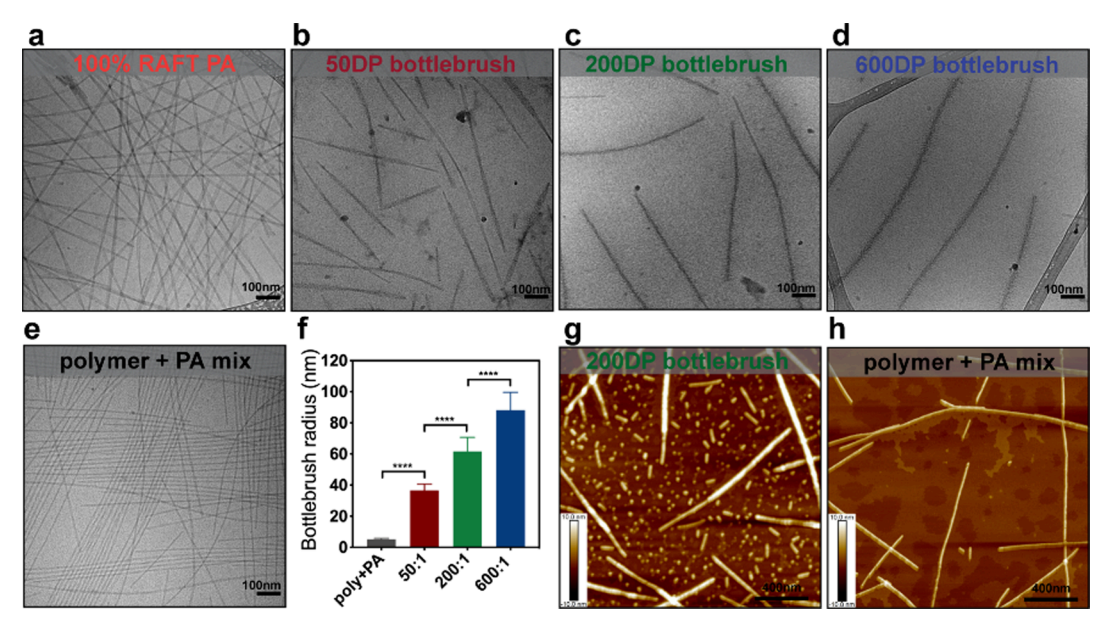


**Figure 2.** Hybrid bonding bottlebrush polymers. Representative cryoTEM micrographs of (a) 100% RAFT PA without polymer grafting and poly(sodium 4-styrenesulfonate) grafted from 100% RAFT PA supramolecular polymers at a monomer/CTA ratio of (b) 50:1, (c) 200:1, and (d) 600:1. (e) CryoTEM micrograph of poly(sodium 4-styrenesulfonate) polymerized in the presence of the unfunctionalized diluent supramolecular polymers using free, soluble BTPA CTA (mixture). (f) Quantification of bottlebrush radii measured from representative cryoTEM micrographs at different monomer/CTA ratios and for the polymer + diluent PA mixture. Significance assessed by one-way ANOVA and a Bonferroni posthoc test, \*\*\*\*P < 0.0001,  $n_{min} = 20$  per group. Representative atomic force microscopy height micrographs of (g) the 200DP bottlebrush and (h) the Polymer + PA mixture.

polymers, where the grafted chains form through covalent bonds but the backbone is formed by noncovalent bonding among monomers.

Hybrid Bonding Bottlebrush Polymers. Following the successful incorporation of chain transfer agent functionality into supramolecular polymers, we next investigated the ability to graft covalent polymers from these assemblies to create hybrid bonding bottlebrush polymers. Aqueous PET-RAFT polymerization was initially performed from supramolecular polymers consisting of 100% RAFT PA as the backbone in order to achieve a high grafting density in the bottlebrush architecture. PET-RAFT polymerization was chosen because previous reports have shown it to be highly amenable to aqueous conditions, suitable for a wide range of monomer classes, and able to achieve rapid polymerization rates at ambient temperatures. 43-48 These properties make this type of polymerization ideal for use in conjunction with water-soluble supramolecular polymers. Covalent polymer brushes of poly(sodium 4-styrenesulfonate) (p(NaSS)) were grown from the supramolecular polymer backbone using the method described in the Supporting Information in order to create a dense bottlebrush architecture with highly charged sulfonated covalent chains (Figure 2). NaSS was chosen as an ideal monomer to investigate this hybrid bonding bottlebrush approach due to its water solubility and overall anionic charge so that it would not interfere with the negatively charged supramolecular polymer assembly. The selection of this monomer was also important for contrast purposes in cryoTEM imaging. NMR analysis indicated that a nearly complete conversion of monomer was achieved after 4 h of polymerization at all chain transfer agent (CTA) to monomer ratios tested, grafting from the 100% RAFT agent PAfunctionalized supramolecular polymers (monomer/CTA of 50:1 (50 DP), 200:1 (200 DP), and 600:1 (600 DP), Figure S6). Aqueous gel permeation chromatography with multiangle

light scattering detection (GPC-MALS) was used to determine the molecular weight of the polymer brushes. This was achieved by analyzing p(NaSS) polymerized under conditions identical to those of free BTPA in solution (rather than the RAFT PA supramolecular polymer) as an approximation for the grafted polymers in the hybrid bonding bottlebrush architecture. We initially attempted to characterize the complete hybrid bonding bottlebrush architecture by GPC-MALS; however, the heterogeneity of the hybrid bonding polymer and the noncovalently bonded backbone made this challenging. When targeting 50:1, 200:1, and 600:1 monomer/ CTA ratio, the molecular weight  $(M_w)$  observed in all cases was higher than the  $M_n$  values predicted by theory, with polydispersities of 1.54, 1.31, and 1.22, respectively (Table S2 and Figure S7). The observed molecular weight exceeding theoretical predictions is likely a result of inefficient initiation of the RAFT CTAs in our polymerization system or early termination of small oligomers. UV-vis spectroscopy of purified polymer showed an absorbance peak at 315 nm resulting from the trithiocarbonate chain transfer agent, confirming chain end fidelity was maintained throughout the polymerization process (Figure S3).

CryoTEM imaging revealed the formation of micrometer-length bottlebrush architectures with a dense p(NaSS) brush corona grafted from the supramolecular backbone. The electron density of the aromatic NaSS provided high contrast by cryoTEM and direct observation of the bottlebrush architecture (Figure 2a-d). Interestingly, when targeting low DP brushes (i.e., 50DP) the supramolecular backbone was able to maintain a twisted nanoribbon morphology (Figure 2b). However, when targeting larger grafted chains from the backbone (i.e., 200 or 600 DP, Figure 2c,d), the twisted nanoribbon architecture was less pronounced, suggesting the length of the covalent polymers impeded this backbone twisting, possibly a result of enhanced covalent polymer

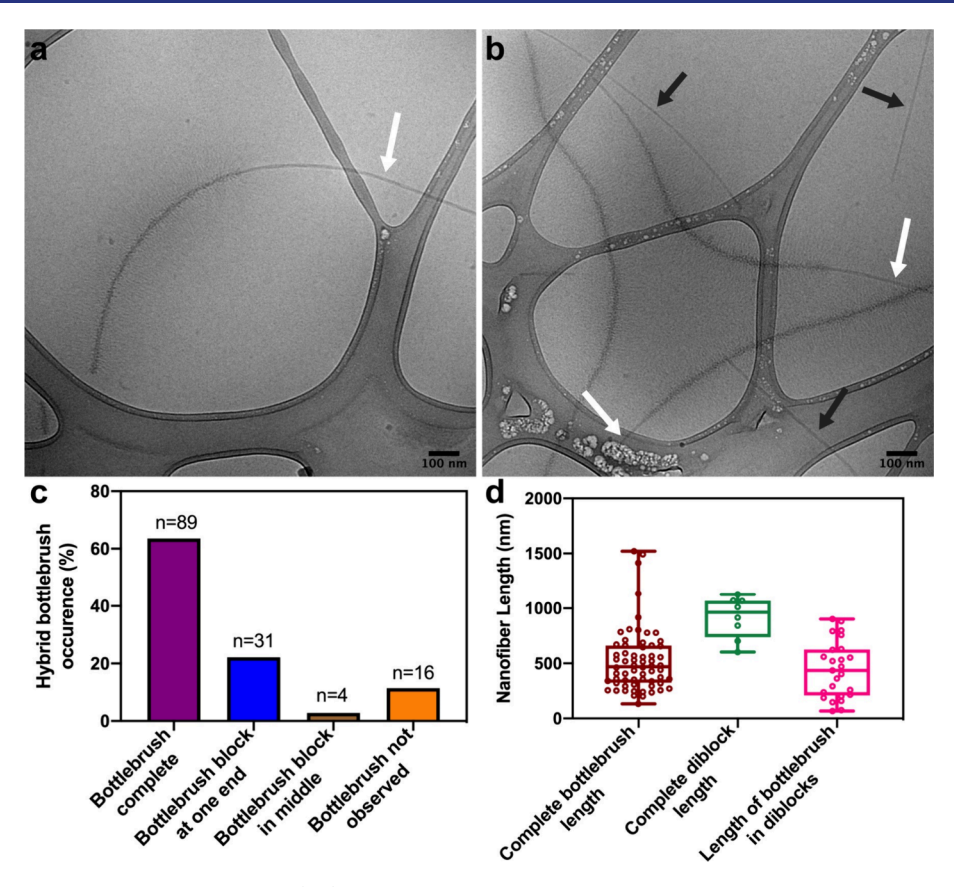


Figure 3. Heterogeneity in bottlebrush architecture. (a,b) CryoTEM micrographs of the 600DP bottlebrush architecture polymerized from 100% RAFT PA supramolecular polymers with white arrows indicating block regions without an observable polymer brush and black arrows indicating supramolecular polymers without grafted p(NaSS) brushes along their length. (c) Percentage quantification of assemblies observed by cryoTEM of the 200DP bottlebrush architecture including the bottlebrush completely covering the supramolecular backbone, blocky at one end, observed in the middle, or not visible at all. (d) Box and whisker plots (box defined as 25% and 75% quartile with midline as median, whiskers as minimum and maximum value respectively) comparing observed length of the complete bottlebrush assembly, to the complete diblock structure, and measured length of the bottlebrush blocks within the diblock structures.

brush entanglements. Importantly, the elongated bottlebrush architectures (observed lengths up to approximately 1  $\mu$ m) demonstrated that the process of polymerization did not disrupt the supramolecular polymer assembly. In addition, polymerization from untethered BTPA in the presence of the unfunctionalized diluent PA supramolecular polymers (mixture) also did not disrupt the supramolecular polymer assembly (Figure 2e). Interestingly, we did not observe a brush architecture by cryoTEM when polymerization of p(NaSS) took place in the presence of free BTPA and unfunctionalized PA supramolecular polymers. This confirms the importance of tethering the RAFT agent covalently to the supramolecular backbone in order to generate the hybrid bonding bottlebrush architecture. Measurements of the hybrid bonding bottlebrush radii revealed a monotonic increase in the brush length with an increasing targeted degree of polymerization (DP), demonstrating control over the covalent brush length during the polymerization (Figure 2f). Atomic force microscopy (AFM) of the hybrid bonding bottlebrush indicated considerably larger (taller and wider) structures in the bottlebrush sample compared to those in the mixture of PA and polymer (Figure 2g,h). Furthermore, short structures in the bottlebrush sample were observed, which we attribute to supramolecular backbone disassembly occurring during drying of these samples for AFM analysis. AFM also allowed us to investigate both tip adhesion and energy dissipation characteristics of the materials. For the bottlebrush sample, significant energy dissipation was observed in the regions containing polymer surrounding the supramolecular backbone, indicative of a soft polymer corona surrounding a relatively stiffer supramolecular polymer core (Figure S8). This difference in material stiffness was not observed in the mixture of PA and polymer, where regions of PA and amorphous flat areas of polymer on the drying film are distinctly observed as separate components (Figure S8).

A Nile red assay was used to probe the critical aggregation concentration (CAC) of the supramolecular polymer backbone before and after the process of covalent polymerization to measure how the grafted polymer affects supramolecular polymerization. The fluorescence from Nile red, a solvatochromic fluorescent dye, is significantly enhanced when in hydrophobic environments like those observed in the core of PA supramolecular assemblies. 42,49 The CAC for the 100% RAFT PA supramolecular polymer was 4.6  $\mu$ M (Figure S9). Following polymerization of sodium 4-styrenesulfonate from the RAFT-functionalized supramolecular polymer backbone at a 200:1 or 600:1 monomer/CTA ratio resulted in a measured CAC of 9.5 and 7.2  $\mu$ M, respectively (Figure S9). As anticipated, Nile Red fluorescence was not observed from the hydrophilic p(NaSS) polymer alone (Figure S9). Taken together, these results suggest that the process of grafting covalent polymers from the supramolecular polymer assembly

does not affect the ability of the molecules to form a hydrophobic core, an important parameter in the supramolecular polymerization of these molecules. To investigate this further, a sample of the 200:1 hybrid bonding bottlebrush polymer was diluted below the CAC (2  $\mu$ M) and imaged by cryoTEM, and as expected we did not observe any structures (Figure S10).

In order to further visualize the bottlebrush architecture, confocal microscopy was used to probe the colocalization of the p(NaSS) covalent polymer brush with the supramolecular polymer backbone. To achieve this, the RAFT PA supramolecular polymer was doped with 1 mol % of a carboxytetramethylrhodamine labeled diluent PA to allow for visualization of the supramolecular polymer backbone while 1 wt % 7-[4-(trifluoromethyl)coumarin]acrylamide was covalently incorporated during the covalent polymerization of sodium 4-styrenesulfonate for visualization of the polymer brush. In discrete fiber-like structures we observed significant colocalization between the fluorescently labeled components of the hybrid bonding bottlebrush architecture, consistent with dimensions obtained from both cryoTEM and AFM (Figure S11). In contrast, control experiments where the polymer was grown from free BTPA in the presence of the diluent supramolecular polymer appeared to form large amorphous regions of colocalization without any fibers (Figure S11). This formation was potentially driven by hydrophobic interactions between the respective dye labels and was not evident in hybrid bonding bottlebrush samples.

Even when all the monomers of PA supramolecular polymers were functionalized with a RAFT CTA functionality, the grafting of polymer side chains was not observed to be homogeneous across the assemblies as observed by cryoTEM. Some supramolecular polymers displayed a block of densely packed covalent brushes and a block without any apparent grafted polymer, while others displayed no evidence of polymer grafted from the supramolecular backbone at all (Figure 3). Inefficient initiation and rapid termination have been reported in other systems using controlled radical polymerization to graft from surfaces as a result of molecular surface crowding.<sup>50</sup> However, we would anticipate that in our system, this would result in a random distribution of polymers grafted from the supramolecular backbone. We propose the "blocky" brush architecture observed in our system is partly the result of the inefficient initiation but most importantly to the dynamic behavior of monomers that is possible within supramolecular polymers. 51-53 We hypothesize that such dynamic behavior also allows internal translational motion within the supramolecular polymers, leading to spatial reorganization of polymer chain-grafted PA monomers into densely packed arrangements observable by cryoTEM. An important consideration of the stability of the bottlebrush architecture was to ensure this was not solely a kinetically trapped state. To probe this further, an aliquot of the hybrid bottlebrush was annealed at 80 °C for 30 min before being allowed to slowly cool back to room temperature over several hours to allow the system to approach thermodynamic equilibrium. CryoTEM imaging following this second annealing (i.e., once prior to and once after covalent polymerization) demonstrated the bottlebrush architecture was maintained, suggesting this is a thermodynamically stable architecture (Figure S12).

In order to better understand our observations, we aimed to quantify p(NaSS) grafting from the supramolecular nanofibers

by analyzing 140 unique hybrid bonding bottlebrush nanofibers from 35 separate cryoTEM micrographs of the 200DP hybrid bonding bottlebrush architecture (Figure 3). We observed that 64% of the bottlebrushes were completely covered with densely grafted brushes, 22% had a single region of densely packed polymer brushes connected to the supramolecular polymer without any grafted polymer chains, 3% with a block of brush in the middle of a supramolecular polymer, and 11% did not reveal any evidence of covalent brush grafting. Similar trends in the distribution of the architectures were also observed for the 600DP hybrid bonding bottlebrush architectures (Figure S13). It is worth noting that the small fields of view in cryoTEM are often not large enough to observe the entire length of the supramolecular polymer assemblies. Finally, we did not see any evidence of multiblock structures (i.e., two or more regions of brushes grafted from the same supramolecular polymer), suggesting that this could be a thermodynamically unfavorable configuration. We believe that the "blockiness" is the result of two driving forces within the hybrid bonding polymer system. The first is the potential for favorable packing among the grafted covalent polymer chains, resulting from both hydrophobic aromatic interactions of styrene residues in the p(NaSS) and the entropically favorable exclusion of water bound to sulfonate groups achieved during this tight packing of polymer chains. This exclusion of water by grafted polymer is further supported by the relatively high degree of contrast in cryoTEM for the dense brush architecture.

It is also possible that the p(NaSS) grafted supramolecular monomers are segregated into a blocky hybrid structure. This results in the self-organization of a rigid block that benefits from a lower enthalpy originating in interactions among graft segments and a much more dynamic supramolecular polymer segment with higher entropy. The system can achieve this selforganized binary population of molecules because of the characteristic dynamics of supramolecular polymers. Mechanistically this could involve either translation of monomers along the length of the hybrid bonding polymer or exchange of monomers among the assemblies. Analysis of the overall length of the bottlebrush hybrid bonding polymers (i.e., covalent brushes observed along the entire supramolecular backbone) versus the diblock structures (i.e., a portion of the supramolecular polymer backbone contains bottlebrush architecture and the remainder appears to contain only supramolecular backbone) demonstrates that the dense bottlebrush segments are shorter compared to the diblock architectures (Figure 3d). We hypothesize this could be a result of the mismatch in hybrid supramolecular polymer dynamics, leading to a critical point that in turn results in rupture of the bottlebrush portion from the ungrafted supramolecular polymer (Figure 3d). This would also explain why we observe supramolecular polymers in the system without bottlebrush architecture at all (black arrows in Figure 3b). Based on the statistical analysis of cryoTEM micrographs, we conclude that the dominant structure in the system investigated is the homogeneous bottlebrush hybrid bonding polymer (64% of structures). An important factor to improve overall yield of hybrid bottlebrush architecture might require a more efficient covalent polymerization of the graft. Another possible direction to address this issue could explore changes in chemical structure of the monomers forming the supramolecular polymer to tailor dynamics and in this way enhance further the overall yield of the bottlebrush hybrid architecture. 52-54

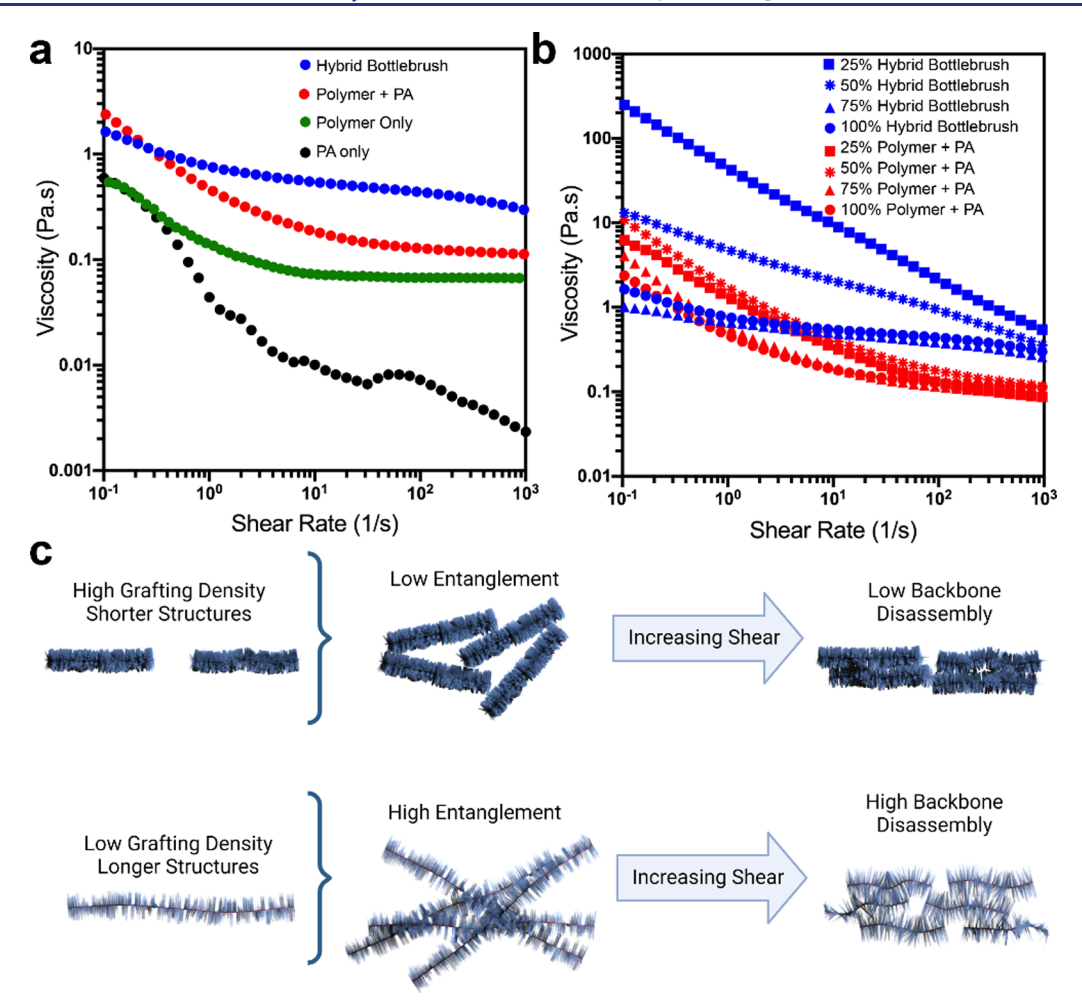
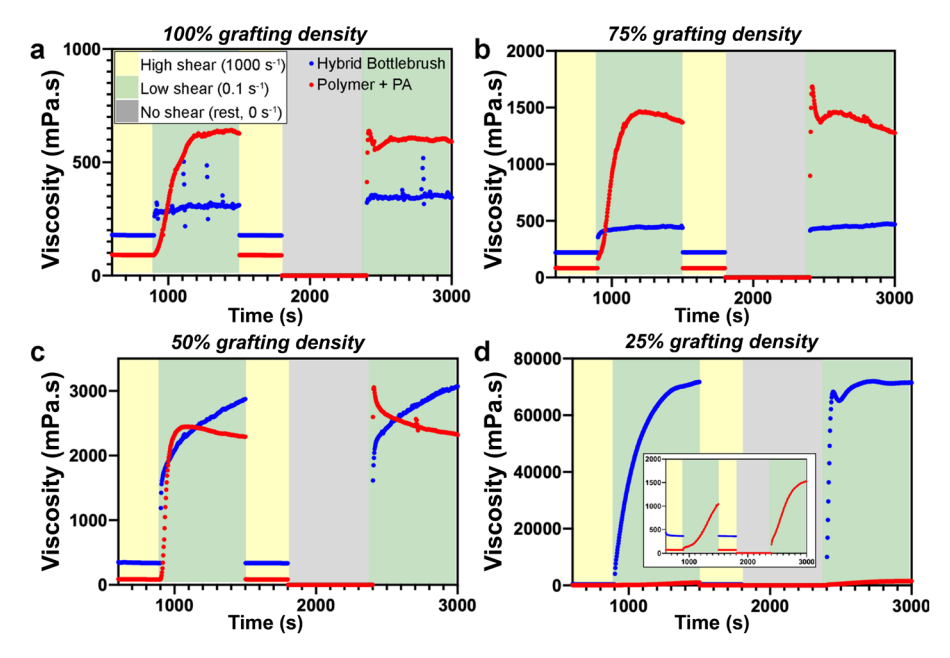


Figure 4. Sample viscosity as a function of shear rate. (a) Flow curve of the 600DP target poly(sodium 4-styrenesulfonate) brush length hybrid bonding bottlebrush (20 wt %, blue), Polymer + PA mixture (600DP target poly(sodium 4-styrenesulfonate) with 1.6 mM diluent PA, 20 wt %, red), polymer alone (600DP target poly(sodium 4-styrenesulfonate), 20 wt %, green) and PA alone (1.6 mM diluent PA, black) (all samples were prepared in water). (b) Comparison of sample viscosity for various grafting densities for the 600DP hybrid bonding bottlebrush (25, 50, 75, and 100% grafting density, 20 wt %, blue) and the corresponding polymer and PA mixtures (20 wt %, red). (c) Schematic representation of the differences contributing to the change in solution viscosity with shear for varied brush grafting density in the hybrid bonding bottlebrush.

Rheological Properties of Hybrid Bonding Bottlebrushes. Initially we investigated the impact of different parameters including brush grafting density, brush molecular weight, and ionic strength on sample viscosity. The dependence of sample viscosity on shear rate (flow curve) was determined for the hybrid bonding bottlebrush and compared to a mixture combining p(NaSS) with the diluent PA supramolecular polymer at the same ratios as the bottlebrush (polymer and PA mixture), p(NaSS) alone, and PA supramolecular polymer alone (Figure 4a). The bottlebrush sample had the highest sample viscosity across the shear rates tested, with mild shear thinning behavior observed. The overall increase in viscosity was likely due to the greater charge density and bulkiness of the bottlebrush structures. The mixture of PA and polymer displayed shear thinning behavior until a shear rate of approximately 5 s<sup>-1</sup>; above 5 s<sup>-1</sup>, the viscosity remained relatively independent of shear rate and matched the p(NaSS) polymer alone as the polymer started to dominate the flow behavior. The PA alone sample (i.e., no p(NaSS)) has a significantly lower viscosity at moderate to high shear rates than the other samples due to a pronounced shear thinning behavior, likely the result of supramolecular polymer disassembly at high shear rates (Figure 4a). Taken together,

these data suggest that the covalent polymer in the bottlebrush architecture prevented the supramolecular backbone from disassembly at high shear rates.

The effect of concentration on flow behavior was compared between the hybrid bonding bottlebrush and the mixture of PA and polymer without the bottlebrush architecture (Figure S14). As anticipated, the viscosity of the solutions scaled linearly with concentration for both the hybrid bottlebrush and the mixture of polymer and PA. However, the bottlebrush sample exhibited a greater rate of viscosity change as a function of concentration compared to the mixture of PA and polymer. The rate of change in viscosity of the hybrid bottlebrush was 6.5 times greater at low shear rates (1 s<sup>-1</sup>) and three times greater at high shear rates (960 s<sup>-1</sup>) compared to the concentration-dependent viscosity changes of the PA and polymer mixture (Figure S14). Furthermore, the viscosity measured at a high shear rate at all concentrations was greater for the bottlebrush relative to the corresponding mixture of PA and polymer at the same concentration (Figure S14). Interestingly, the addition of different salts had a minimal effect on the sample viscosity within the shear range tested (Figure S15). We propose that this is due to the strong binding of sodium ions to the sulfonate groups of the p(NaSS) during



**Figure 5.** Thixotropy analysis of hybrid bottlebrush with varying degrees of grafting density. Solution viscosity for the 600DP targeted poly(sodium 4-styrenesulfonate) bottlebrush (hybrid bottlebrush, blue) and equivalent poly(sodium 4-styrenesulfonate) mixture with supramolecular polymer (polymer + PA, red), for (a) 100%, (b) 75%, (c) 50%, and (d) 25% (inset highlights low viscosity sample response) grafting density. Samples were subjected to a period of high shear (yellow shading, 1000 s<sup>-1</sup>), low shear (green shading, 0.1 s<sup>-1</sup>), repeated high shear, no shear (gray shading, 0 s<sup>-1</sup>), and finally repeated low shear. All samples were prepared to a final 20 wt % solution in water.

synthesis, which avoids electrostatic repulsion. This is supported by the fact that further addition of either monovalent or divalent cations does not significantly alter these tightly bound ions and hence the observed minimal changes in sample viscosity. We further explored the role of brush molecular weight on the rheological properties of the hybrid bottlebrush compared to the polymer and PA mixture without bottlebrush architecture (Figure S15). When varying the degree of polymerization from a target of 200DP p(NaSS) brush to a 600DP target, we did not see any appreciable difference in the measured viscosity of the samples compared to observations made when varying the overall sample concentration.

To compare grafting density, supramolecular polymers were formed through molecular coassembly of the RAFT PA and the diluent PA to achieve backbones with varying amounts of RAFT CTA functionality (25, 50, and 75 mol % RAFT PA) as described in Figure 1. Covalent brushes of p(NaSS) were then polymerized from these supramolecular backbones following the same methods described for the 100% RAFT PA supramolecular polymer. However, observations by cryoTEM demonstrated that although bottlebrushes were still present in all samples, the ratio of observed dense bottlebrush regions relative to supramolecular polymer regions without brushes also decreased as the RAFT PA content in the coassembly was decreased (Figure S16). Again, this is a likely result of the dynamic capabilities of the supramolecular polymer backbone to reorganize at the molecular level. The flow properties of the hybrid bottlebrush were significantly altered as a result of grafting density, with lower grafting densities resulting in much higher viscosities at low to moderate shear rates compared to the mixture of polymer and PA (Figure 4b). These differences we believe are a result of greater entanglement at low shear facilitated by the longer structures achieved at low brush grafting densities compared to the shorter structures with high brush grafting densities. As shear increases, the supramolecular

backbone is less protected in bottlebrushes with low grafting density and can in turn disassemble into smaller segments to achieve viscosities similar to those observed with 100% grafting (Figure 4c). This provides further evidence that the presence of the covalent polymer brushes is able to impart protection to the supramolecular polymer backbone against shear induced disassembly.

We next used a thixotropy test to further understand the mechanism governing the viscosity differences observed with hybrid bonding bottlebrushes of different polymer grafting density. Solutions of the hybrid bottlebrush and the mixture of polymer and PA were subjected to periods of high shear, low shear, and no shear at all to observe how viscosity changed with respect to time under these conditions (Figure 5). Under high shear, all grafting densities of the hybrid bonding bottlebrush showed a greater solution viscosity compared with the polymer and PA mixture, consistent with our observations in Figure 4b. During periods of low shear following this high shear event, low bottlebrush grafting densities (50% and 25%) and the polymer and PA mixtures at all conditions exhibited increasing viscosity with time, indicative of supramolecular polymer healing, elongation, and resulting re-entanglement (Figure 5). This behavior was not observed with the 100% and 75% grafting density hybrid bottlebrush samples, which demonstrated a higher viscosity but a constant viscosity plateau during the low shear (Figure 5a,b). This supports our hypothesis that at high grafting density, the dense covalent polymer brush network can protect the supramolecular backbone from disassembly at high shear. When the polymer grafting density is low (below 50%), the self-healing capabilities are maintained for the supramolecular backbone of the hybrid bottlebrush following high shear. This was supported with TEM imaging of the bottlebrush samples following low shear recovery at the completion of the thixotropy test, where it is evident that the recovered hybrid bottlebrush architecture results in longer structures at lower

grafting densities (Figure S17). The self-healing of the supramolecular backbone was evident, after a period of rest (no shear), during which recovery could occur and under subsequent low shear viscosity again increased with time to similar values observed during the first period of low shear in all cases. This demonstrates that a high degree of recovery for the low grafting hybrid bonding bottlebrush architectures is possible, while maintaining the increased viscosity resulting from bottlebrush architecture.

Following the viscosity assessment, we wanted to probe the mechanical properties of the bottlebrush architecture at different brush grafting densities through measurement of storage (G') and loss (G'') moduli as a function of strain. In all cases, the critical strain value  $(\gamma_c)$ , the strain at which the storage modulus begins to dramatically decrease, occurs at lower strain for the mixture of polymer and PA relative to the hybrid bottlebrush architecture (Figure 6). When comparing

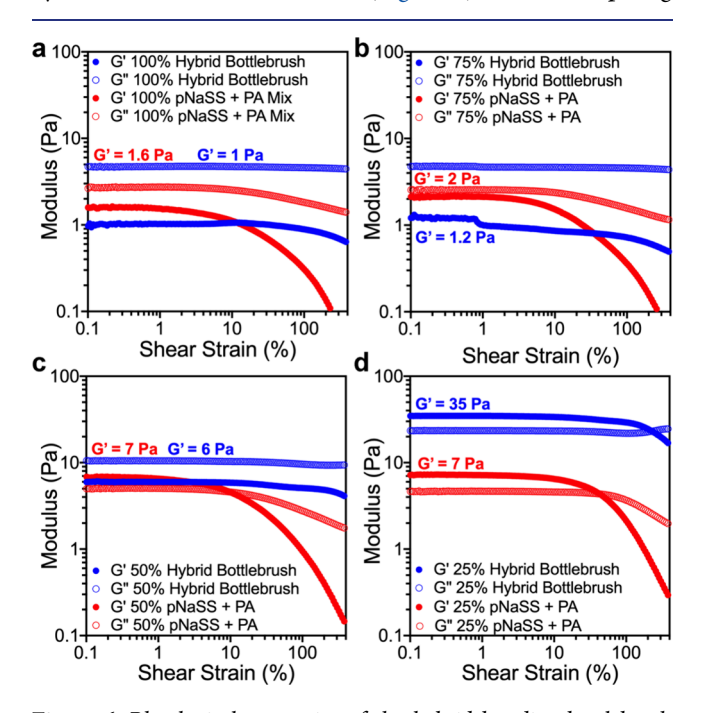


**Figure 6.** Rheological properties of the hybrid bonding bottlebrush architecture. Storage (G', closed circles) and loss moduli (G'', open circles) as a function of shear strain (strain sweep) for the 600DP targeted poly(sodium 4-styrenesulfonate) bottlebrush (hybrid bottlebrush, blue) and equivalent poly(sodium 4-styrenesulfonate) mixture with supramolecular polymer (polymer + PA, red), for (a) 100%, (b) 75%, (c) 50%, and (d) 25% grafting density. All samples were prepared to a final 20 wt % solution in water.

the brush grafting densities, the 25% bottlebrush exhibits a storage modulus above the loss modulus (G' > G'') across most of the shear range tested, whereas samples with higher grafting density all exhibited the loss moduli exceeding that of the storage modulus (Figure 6). The strain sweep was performed at an angular frequency of 10 rad/s, so the observed relationships between storage and loss moduli were consistent with the frequency sweep (Figure S18). Also of interest is that the storage modulus for the 25% hybrid bottlebrush in the linear viscoelastic range (LVER) is approximately five times that of the mixture containing equivalent polymer and PA. In comparison, all of the higher grafting density hybrid bottlebrush samples demonstrated comparable LVER storage moduli relative to their correspond-

ing mixtures (Figure 6). These results further support the protection of the supramolecular backbone from shear-induced disassembly at high grafting densities. This observation could be interpreted to be the result of a greater internal cohesion in bottlebrush architectures given the favorable interactions among grafted polymer chains.

# CONCLUSIONS

We have developed a synthetic approach to form bottlebrush polymers in an aqueous environment utilizing peptide amphiphile supramolecular polymers as the backbone. To achieve this, we used photoinitiated RAFT polymerization from chain transfer agents tethered to our supramolecular polymer backbones to graft covalent brushes of the watersoluble polymer p(NaSS). We investigated the ability to tune both the grafting density (through supramolecular coassembly) and brush molecular weight in these hybrid bonding polymer systems. Interestingly, grafting of the covalent polymer from the supramolecular backbone results in block bottlebrush architectures with regions of high grafting density observed by cryoTEM combined with regions of no observable brushes, despite all supramolecular monomers capable of grafting polymer chains. We believe this unique finding comes from favorable interactions among densely packed covalent chains but, most importantly, from the dynamic behavior capable of the monomers in the supramolecular polymer backbone. Further analysis of these materials by computational methods could help elucidate the role that this dynamic behavior has on bottlebrush diblock formation. Grafting of covalent polymers from the supramolecular polymer backbone results in higher solution viscosity while also imparting protection from disassembly of the supramolecular backbone, which can be viewed as the result of additional internal cohesion contributed by interactions among the grafted chains. Furthermore, through optimization of grafting density, relatively high solution viscosity can be achieved while maintaining the selfhealing capabilities of peptide amphiphile supramolecular polymers. In principle, the systems investigated here could be simply diluted to a critical aggregation concentration to effectively disassemble the bottlebrush architecture into much lower molecular weight species and a biodegradable supramolecular backbone. Such options could be attractive in the context of using hybrid bonding polymer architectures to address concerns about the life cycle of synthetic soft materials. The specific chemistries explored here may be of interest as aqueous lubricants or viscosity modifiers as well as biomaterials that emulate proteoglycans.

## ASSOCIATED CONTENT

# Supporting Information

The Supporting Information is available free of charge at https://pubs.acs.org/doi/10.1021/jacs.4c03320.

Additional figures at high resolution of the hybrid bonding bottlebrush architectures, description of synthetic procedures, and detailed explanation of materials and methods used (PDF)

## AUTHOR INFORMATION

# **Corresponding Author**

Samuel I. Stupp — Simpson Querrey Institute for BioNanotechnology and Department of Medicine, Northwestern University, Chicago, Illinois 60611, United States; Department of Chemistry, Department of Materials Science and Engineering, and Department of Biomedical Engineering, Northwestern University, Evanston, Illinois 60208, United States; orcid.org/0000-0002-5491-7442; Email: s-stupp@northwestern.edu

## **Authors**

- Tristan D. Clemons Simpson Querrey Institute for BioNanotechnology, Northwestern University, Chicago, Illinois 60611, United States; Department of Chemistry, Northwestern University, Evanston, Illinois 60208, United States; Present Address: Present address: School of Polymer Science and Engineering, The University of Southern Mississippi, Hattiesburg, MS 39401, USA; orcid.org/0000-0001-8042-0141
- Simon A. Egner Department of Materials Science and Engineering, Northwestern University, Evanston, Illinois 60208, United States; orcid.org/0000-0001-9430-7844
- Joseph Grzybek Department of Chemistry, Northwestern University, Evanston, Illinois 60208, United States; orcid.org/0009-0002-5925-8703
- Joshua J. Roan Department of Materials Science and Engineering, Northwestern University, Evanston, Illinois 60208, United States
- Hiroaki Sai Simpson Querrey Institute for BioNanotechnology, Northwestern University, Chicago, Illinois 60611, United States; orcid.org/0000-0002-4268-2148
- Yang Yang Simpson Querrey Institute for BioNanotechnology, Northwestern University, Chicago, Illinois 60611, United States; orcid.org/0000-0003-2409-5529
- Zois Syrgiannis Simpson Querrey Institute for BioNanotechnology, Northwestern University, Chicago, Illinois 60611, United States; Department of Chemistry, Northwestern University, Evanston, Illinois 60208, United States
- Hao Sun Simpson Querrey Institute for BioNanotechnology, Northwestern University, Chicago, Illinois 60611, United States; International Institute of Nanotechnology, Chemistry of Life Processes Institute, Northwestern University, Evanston, Illinois 60208, United States; orcid.org/0000-0001-9153-4021
- Liam C. Palmer Simpson Querrey Institute for BioNanotechnology, Northwestern University, Chicago, Illinois 60611, United States; Department of Chemistry, Northwestern University, Evanston, Illinois 60208, United States; orcid.org/0000-0003-0804-1168
- Nathan C. Gianneschi Simpson Querrey Institute for BioNanotechnology, Northwestern University, Chicago, Illinois 60611, United States; Department of Chemistry, Department of Materials Science and Engineering, Department of Biomedical Engineering, Department of Pharmacology, and International Institute of Nanotechnology, Chemistry of Life Processes Institute, Northwestern University, Evanston, Illinois 60208, United States; orcid.org/0000-0001-9945-5475

Complete contact information is available at: https://pubs.acs.org/10.1021/jacs.4c03320

## **Author Contributions**

The manuscript was written through contributions of all authors. All authors have given approval to the final version of the manuscript.

## **Funding**

This work was primarily supported by the National Science Foundation under grant DMR-2310178. Additional support was provided by the National Science Foundation CHE-2102662 (for NMR spectroscopy studies) and by the Center for Regenerative Nanomedicine at the Simpson Querrey Institute for BioNanotechnology at Northwestern University (for the mechanical testing). T.DC. acknowledges funding support from an American Australian Association Fellowship.

## Notes

The authors declare no competing financial interest.

# ACKNOWLEDGMENTS

We are grateful to the following core facilities at Northwestern University: Peptide Synthesis Core at the Simpson Querrey Institute, supported by the Soft and Hybrid Nanotechnology Experimental (ShyNE) Resource (NSF ECCS - 1542205). The Simpson Querrey Institute, Northwestern University Office for Research, U.S. Army Research Office, and the U.S. Army Medical Research and Materiel Command have also provided funding to develop this facility. Circular dichroism spectroscopy was performed at the Northwestern University Keck Biophysics facility, which is generously supported by an NCI Cancer Center Support Grant (P30 CA060553) awarded to the Robert H Lurie Comprehensive Cancer Center. Electron microscopy experiments were performed at the Electron Probe Instrumentation Center (EPIC) and the BioCryo facility of Northwestern University's NUANCE Center, which have both received support from the Soft and Hybrid Nanotechnology Experimental (ShyNE) Resource (NSF ECCS-1542205); the MRSEC program (NSF DMR-1720139) at the Materials Research Center; the International Institute for Nanotechnology (IIN); the Keck Foundation; and the State of Illinois, through the IIN. NMR and FTIR characterization in this work made use of IMSERC at Northwestern University, which has received support from the Soft and Hybrid Nanotechnology Experimental (ShyNE) Resource (NSF ECCS-1542205), the State of Illinois, and the International Institute for Nanotechnology (IIN). Rheology experiments made use of the MatCI Facility supported by the MRSEC program of the National Science Foundation (DMR-1720139) at the Materials Research Center of Northwestern University. Portions of this work were performed at the DuPont-Northwestern-Dow Collaborative Access Team (DND-CAT) located at Sector 5 of the Advanced Photon Source (APS). DND-CAT is supported by Northwestern University, The Dow Chemical company, and DuPont de Nemours, Inc. This research used resources of the Advanced Photon Source, a U.S. Department of Energy (DOE) Office of Science User Facility operated for the DOE Office of Science by Argonne National Laboratory under Contract No. DE-AC02-06CH11357. Cinema 4D illustrations were created by Mark Seniw in the Analytical bioNanoTechnology Equipment Core Facility of the Simpson Querrey Institute for BioNanotechnology at Northwestern University, with partial support from the Soft and Hybrid Nanotechnology Experimental (SHyNE) Resource (NSF ECCS-2025633). Parts of this work were carried out at the Soft Matter Characterization

Facility of the University of Chicago and the authors are thankful to the help provided by Philip Griffin in obtaining this data. The authors would like to thank Kristen Wek and Jacob Kupferberg for help with scanning electron microscopy and rheology experiments respectively, and Mark Seniw for his design of Cinema 4D schematic drawings in the manuscript.

# REFERENCES

- (1) Lee, H. I.; Pietrasik, J.; Sheiko, S. S.; Matyjaszewski, K. Stimuliresponsive molecular brushes. Prog. Polym. Sci. 2010, 35 (1-2), 24-44.
- (2) Sheiko, S. S.; Sumerlin, B. S.; Matyjaszewski, K. Cylindrical molecular brushes: Synthesis, characterization, and properties. Prog. Polym. Sci. 2008, 33 (7), 759-785.
- (3) Yan, J. J.; Bockstaller, M. R.; Matyjaszewski, K. Brush-modified materials: Control of molecular architecture, assembly behavior, properties and applications. Prog. Polym. Sci. 2020, 100, No. 101180.
- (4) Gubbiotti, M. A.; Vallet, S. D.; Ricard-Blum, S.; Iozzo, R. V. Decorin interacting network: A comprehensive analysis of decorinbinding partners and their versatile functions. Matrix Biol. 2016, 55, 7 - 21.
- (5) Christensen, G.; Herum, K. M.; Lunde, I. G. Sweet, yet underappreciated: Proteoglycans and extracellular matrix remodeling in heart disease. Matrix Biol. 2019, 75-76, 286-299.
- (6) Xia, Y. Q.; Adibnia, V.; Huang, R. L.; Murschel, F.; Faivre, J.; Xie, G. J.; Olszewski, M.; De Crescenzo, G.; Qi, W.; He, Z. M.; et al. Biomimetic Bottlebrush Polymer Coatings for Fabrication of Ultralow Fouling Surfaces. Angew. Chem. Int. Edit 2019, 58 (5), 1308-1314.
- (7) Radzinski, S. C.; Foster, J. C.; Chapleski, R. C.; Troya, D.; Matson, J. B. Bottlebrush Polymer Synthesis by Ring-Opening Metathesis Polymerization: The Significance of the Anchor Group. J. Am. Chem. Soc. 2016, 138 (22), 6998-7004.
- (8) Johnson, J. A.; Lu, Y. Y.; Burts, A. O.; Lim, Y. H.; Finn, M. G.; Koberstein, J. T.; Turro, N. J.; Tirrell, D. A.; Grubbs, R. H. Core-Clickable PEG-Branch-Azide Bivalent-Bottle-Brush Polymers by ROMP: Grafting-Through and Clicking-To. J. Am. Chem. Soc. 2011, 133 (3), 559-566.
- (9) Xie, G. J.; Martinez, M. R.; Olszewski, M.; Sheiko, S. S.; Matyjaszewski, K. Molecular Bottlebrushes as Novel Materials. Biomacromolecules 2019, 20 (1), 27-54.
- (10) Shanmugam, S.; Cuthbert, J.; Kowalewski, T.; Boyer, C.; Matyjaszewski, K. Catalyst-Free Selective Photoactivation of RAFT Polymerization: A Facile Route for Preparation of Comblike and Bottlebrush Polymers. Macromolecules 2018, 51 (19), 7776-7784.
- (11) Bernard, J.; Favier, A.; Davis, T. P.; Barner-Kowollik, C.; Stenzel, M. H. Synthesis of poly(vinyl alcohol) combs via MADIX/ RAFT polymerization. Polymer 2006, 47 (4), 1073-1080.
- (12) Banquy, X.; Burdynska, J.; Lee, D. W.; Matyjaszewski, K.; Israelachvili, J. Bioinspired Bottle-Brush Polymer Exhibits Low Friction and Amontons-like Behavior. J. Am. Chem. Soc. 2014, 136 (17), 6199-6202.
- (13) Faivre, J.; Shrestha, B. R.; Burdynska, J.; Xie, G.; Moldovan, F.; Delair, T.; Benayoun, S.; David, L.; Matyjaszewski, K.; Banquy, X. Wear Protection without Surface Modification Using a Synergistic Mixture of Molecular Brushes and Linear Polymers. ACS Nano 2017, 11 (2), 1762–1769.
- (14) Xia, Y. Q.; Adibnia, V.; Shan, C. C.; Huang, R. L.; Qi, W.; He, Z. M.; Xie, G. J.; Olszewski, M.; De Crescenzo, G.; Matyjaszewski, K.; et al. Synergy between Zwitterionic Polymers and Hyaluronic Acid Enhances Antifouling Performance. Langmuir 2019, 35 (48), 15535-15542.
- (15) Mullner, M.; Dodds, S. J.; Nguyen, T. H.; Senyschyn, D.; Porter, C. J. H.; Boyd, B. J.; Caruso, F. Size and Rigidity of Cylindrical Polymer Brushes Dictate Long Circulating Properties In Vivo. ACS Nano 2015, 9 (2), 1294-1304.
- (16) Cheng, C.; Qi, K.; Khoshdel, E.; Wooley, K. L. Tandem synthesis of core-shell brush copolymers and their transformation to

- peripherally cross-linked and hollowed nanostructures. J. Am. Chem. Soc. 2006, 128 (21), 6808-6809.
- (17) Johnson, J. A.; Lu, Y. Y.; Burts, A. O.; Xia, Y.; Durrell, A. C.; Tirrell, D. A.; Grubbs, R. H. Drug-Loaded, Bivalent-Bottle-Brush Polymers by Graft-through ROMP. Macromolecules 2010, 43 (24), 10326-10335.
- (18) Zou, J. O.; Jafr, G.; Themistou, E.; Yap, Y.; Wintrob, Z. A. P.; Alexandridis, P.; Ceacareanu, A. C.; Cheng, C. pH-Sensitive brush polymer-drug conjugates by ring-opening metathesis copolymerization. Chem. Commun. 2011, 47 (15), 4493-4495.
- (19) Liao, L. Y.; Liu, J.; Dreaden, E. C.; Morton, S. W.; Shopsowitz, K. E.; Hammond, P. T.; Johnson, J. A. A Convergent Synthetic Platform for Single-Nanoparticle Combination Cancer Therapy: Ratiometric Loading and Controlled Release of Cisplatin, Doxorubicin, and Camptothecin. J. Am. Chem. Soc. 2014, 136 (16), 5896-
- (20) Fouz, M. F.; Mukumoto, K.; Averick, S.; Molinar, O.; McCartney, B. M.; Matyjaszewski, K.; Armitage, B. A.; Das, S. R. Bright Fluorescent Nanotags from Bottlebrush Polymers with DNA-Tipped Bristles. ACS Central Sci. 2015, 1 (8), 431-438.
- (21) Faivre, J.; Shrestha, B. R.; Xie, G.; Delair, T.; David, L.; Matyjaszewski, K.; Banquy, X. Unraveling the Correlations between Conformation, Lubrication, and Chemical Stability of Bottlebrush Polymers at Interfaces. Biomacromolecules 2017, 18 (12), 4002-4010.
- (22) Patel, B. B.; Walsh, D. J.; Kim, D.; Kwok, J.; Lee, B.; Guironnet, D.; Diao, Y. Tunable structural color of bottlebrush block copolymers through direct-write 3D printing from solution. Sci. Adv. 2020, 6 (24), No. eaaz7202.
- (23) Abbasi, M.; Faust, L.; Wilhelm, M. Comb and Bottlebrush Polymers with Superior Rheological and Mechanical Properties. Adv. Mater. 2019, 31 (26), 1806484.
- (24) Schneiderman, D. K.; Hillmyer, M. A. 50th Anniversary Perspective: There Is a Great Future in Sustainable Polymers. Macromolecules 2017, 50 (10), 3733-3750.
- (25) Tournier, V.; Topham, C. M.; Gilles, A.; David, B.; Folgoas, C.; Moya-Leclair, E.; Kamionka, E.; Desrousseaux, M. L.; Texier, H.; Gavalda, S.; Cot, M.; Guémard, E.; Dalibey, M.; Nomme, J.; Cioci, G.; Barbe, S.; Chateau, M.; André, I.; Duquesne, S.; Marty, A.; et al. An engineered PET depolymerase to break down and recycle plastic bottles. Nature 2020, 580 (7802), 216.
- (26) Clemons, T. D.; Stupp, S. I. Design of materials with supramolecular polymers. Prog. Polym. Sci. 2020, 111, No. 101310.
- (27) Stupp, S. I.; Clemons, T. D.; Carrow, J. K.; Sai, H.; Palmer, L. C. Supramolecular and Hybrid Bonding Polymers. Isr J. Chem. 2020, 60 (1-2), 124-131.
- (28) Gruschwitz, F. V.; Klein, T.; Catrouillet, S.; Brendel, J. C. Supramolecular polymer bottlebrushes. Chem. Commun. 2020, 56 (38), 5079-5110.
- (29) Street, S. T. G.; He, Y. X.; Jin, X. H.; Hodgson, L.; Verkade, P.; Manners, I. Cellular uptake and targeting of low dispersity, dual emissive, segmented block copolymer nanofibers. Chem. Sci. 2020, 11 (32), 8394-8408.
- (30) Qiu, H. B.; Hudson, Z. M.; Winnik, M. A.; Manners, I. Multidimensional hierarchical self-assembly of amphiphilic cylindrical block comicelles. Science 2015, 347 (6228), 1329-1332.
- (31) Cai, J.; Li, C.; Kong, N.; Lu, Y.; Lin, G.; Wang, X.; Yao, Y.; Manners, I.; Qiu, H. Tailored multifunctional micellar brushes via crystallization-driven growth from a surface. Science 2019, 366 (6469), 1095-1098.
- (32) Boott, C. E.; Gwyther, J.; Harniman, R. L.; Hayward, D. W.; Manners, I. Scalable and uniform 1D nanoparticles by synchronous polymerization, crystallization and self-assembly. Nat. Chem. 2017, 9 (8), 785-792.
- (33) Klein, T.; Ulrich, H. F.; Gruschwitz, F. V.; Kuchenbrod, M. T.; Takahashi, R.; Hoeppener, S.; Nischang, I.; Sakurai, K.; Brendel, J. C. Overcoming the Necessity of a Lateral Aggregation in the Formation of Supramolecular Polymer Bottlebrushes in Water. Macromol. Rapid Commun. 2020, 2000585.

- (34) Klein, T.; Ulrich, H. F.; Gruschwitz, F. V.; Kuchenbrod, M. T.; Takahashi, R.; Fujii, S.; Hoeppener, S.; Nischang, I.; Sakurai, K.; Brendel, J. C. Impact of amino acids on the aqueous self-assembly of benzenetrispeptides into supramolecular polymer bottlebrushes. *Polym. Chem.* **2020**, *11* (42), 6763–6771.
- (35) Gruschwitz, F. V.; Fu, M. C.; Klein, T.; Takahashi, R.; Higashihara, T.; Hoeppener, S.; Nischang, I.; Sakurai, K.; Brendel, J. C. Unraveling Decisive Structural Parameters for the Self-Assembly of Supramolecular Polymer Bottlebrushes Based on Benzene Trisureas. *Macromolecules* **2020**, *53* (17), 7552–7560.
- (36) Yang, J.; Song, J. I.; Song, Q.; Rho, J. Y.; Mansfield, E. D. H.; Hall, S. C. L.; Sambrook, M.; Huang, F. H.; Perrier, S. Hierarchical Self-Assembled Photo-Responsive Tubisomes from a Cyclic Peptide-Bridged Amphiphilic Block Copolymer. *Angew. Chem. Int. Edit* **2020**, 59 (23), 8860–8863.
- (37) Rho, J. Y.; Cox, H.; Mansfield, E. D. H.; Ellacott, S. H.; Peltier, R.; Brendel, J. C.; Hartlieb, M.; Waigh, T. A.; Perrier, S. Dual self-assembly of supramolecular peptide nanotubes to provide stabilisation in water. *Nat. Commun.* **2019**, *10* (10), 4708.
- (38) Larnaudie, S. C.; Brendel, J. C.; Jolliffe, K. A.; Perrier, S. Cyclic Peptide-Polymer Conjugates: Grafting-to vs Grafting-From. *J. Polym. Sci. Pol Chem.* **2016**, *54* (7), 1003–1011.
- (39) Pashuck, E. T.; Cui, H. G.; Stupp, S. I. Tuning Supramolecular Rigidity of Peptide Fibers through Molecular Structure. *J. Am. Chem. Soc.* **2010**, *132* (17), 6041–6046.
- (40) Hamley, I. W.; Nutt, D. R.; Brown, G. D.; Miravet, J. F.; Escuder, B.; Rodriguez-Llansola, F. Influence of the Solvent on the Self-Assembly of a Modified Amyloid Beta Peptide Fragment. II. NMR and Computer Simulation Investigation. *J. Phys. Chem. B* **2010**, 114 (2), 940–951.
- (41) Yang, H. Y.; Yang, S. N.; Kong, J. L.; Dong, A. C.; Yu, S. N. Obtaining information about protein secondary structures in aqueous solution using Fourier transform IR spectroscopy. *Nat. Protoc.* **2015**, 10, 382–396.
- (42) Klein, M. K.; Kassam, H. A.; Lee, R. H.; Bergmeier, W.; Peters, E. B.; Gillis, D. C.; Dandurand, B. R.; Rouan, J. R.; Karver, M. R.; Struble, M. D.; et al. Development of Optimized Tissue-Factor-Targeted Peptide Amphiphile Nanofibers to Slow Noncompressible Torso Hemorrhage. ACS Nano 2020, 14 (6), 6649–6662.
- (43) Sun, H.; Cao, W.; Zang, N.; Clemons, T. D.; Scheutz, G.; Hu, Z.; Thompson, M.; Liang, Y.; Vratsanos, M.; Zhou, X.; et al. Proapoptotic Peptide Brush Polymer Nanoparticles via Photoinitiated Polymerization-Induced Self-Assembly. *Angew. Chem.* **2020**, *59* (43), 19136–19142.
- (44) McClelland, K. P.; Clemons, T. D.; Stupp, S. I.; Weiss, E. A. Semiconductor Quantum Dots Are Efficient and Recyclable Photocatalysts for Aqueous PET-RAFT Polymerization. *ACS Macro Lett.* **2020**, *9* (1), 7–13.
- (45) Yeow, J.; Chapman, R.; Gormley, A. J.; Boyer, C. Up in the air: oxygen tolerance in controlled/living radical polymerisation. *Chem. Soc. Rev.* **2018**, 47 (12), 4357–4387.
- (46) Phommalysack-Lovan, J.; Chu, Y. Y.; Boyer, C.; Xu, J. T. PET-RAFT polymerisation: towards green and precision polymer manufacturing. *Chem. Commun.* **2018**, *54* (50), 6591–6606.
- (47) Tucker, B. S.; Coughlin, M. L.; Figg, C. A.; Sumerlin, B. S. Grafting-From Proteins Using Metal-Free PET-RAFT Polymerizations under Mild Visible-Light Irradiation. *ACS Macro Lett.* **2017**, 6 (4), 452–457.
- (48) Shanmugam, S.; Xu, J. T.; Boyer, C. Aqueous RAFT Photopolymerization with Oxygen Tolerance. *Macromolecules* **2016**, 49 (24), 9345–9357.
- (49) Chen, C. J.; Liu, G. Y.; Liu, X. S.; Pang, S. P.; Zhu, C. S.; Lv, L. P.; Ji, J. Photo-responsive, biocompatible polymeric micelles self-assembled from hyperbranched polyphosphate-based polymers. *Polym. Chem-Uk* **2011**, *2* (6), 1389–1397.
- (50) Zoppe, J. O.; Cavusoglu Ataman, N.; Mocny, P.; Wang, J.; Moraes, J.; Klok, H. A. Surface-Initiated Controlled Radical Polymerization: State-of-the-Art, Opportunities, and Challenges in

- Surface and Interface Engineering with Polymer Brushes. *Chem. Rev.* **2017**, 117 (5), 4667–4667.
- (51) Wester, J. R.; Lewis, J.; Freeman, R.; Sai, H.; Palmer, L.; Henrich, S.; Stupp, S. Supramolecular Exchange Among Assemblies of Opposite Charge Leads to Hierarchical Structures. *J. Am. Chem. Soc.* **2020**, *142* (28), 12216–12225.
- (52) Freeman, R.; Han, M.; Alvarez, Z.; Lewis, J. A.; Wester, J. R.; Stephanopoulos, N.; McClendon, M. T.; Lynsky, C.; Godbe, J. M.; Sangji, H.; et al. Reversible self-assembly of superstructured networks. *Science* **2018**, *362* (6416), 808–813.
- (53) Edelbrock, A. N.; Clemons, T. D.; Chin, S. M.; Roan, J. J. W.; Bruckner, E. P.; Álvarez, Z.; Edelbrock, J. F.; Wek, K. S.; Stupp, S. I. Superstructured Biomaterials Formed by Exchange Dynamics and Host-Guest Interactions in Supramolecular Polymers. *Adv. Sci.* **2021**, 2004042.
- (54) Wester, J. R.; Lewis, J. A.; Freeman, R.; Sai, H.; Palmer, L. C.; Henrich, S. E.; Stupp, S. I. Supramolecular Exchange among Assemblies of Opposite Charge Leads to Hierarchical Structures. *J. Am. Chem. Soc.* **2020**, *142* (28), 12216–12225.